CFD modeling of cavitation in solenoid valves for diesel fuel injection

N. Kayakol
Bosch Diesel Systems, RBTR Bursa, Turkey

Abstract

Solenoid valve of the injector flow shows characteristics of bubbly flow. In the valve seat region of solenoid valves the expansion of fuel flow from high pressure to low pressure regions creates bubbles. Two-phase flow characteristics of ball type solenoid valve for diesel common rail injectors are modelled with mixture model approach, which is suited for bubble–liquid flow. The cavitation model is based on the Rayleigh–Plesset equation. The flow pattern of valve geometry can be considered as high speed jet flow which occurs after throttling of high pressure fuel. The SST turbulence model is used to handle vortex formation. In solenoid valves the mass flow rate control with a throttling pipe and then expansion of jet flow in a diffuser cause bubble generation due to flow detachment and vortex formation, where pressure drops below vapour pressure of fuel. This results in cavitation erosion damage. The quantification of the erosive potential of collapsing vapour structures is done with a cavitation erosion index based on work hardening process. The pressure rise due to the impact of a microjet is estimated from classic water hammer approach. It is shown that cavitation model is very sensitive to condensation rate constant and density ratio of diesel and diesel vapour.
Keywords: cavitation, multiphase, computational fluid dynamics, solenoid valve.

1 Introduction

With fuel prices on the rise and increasingly stricter emission standards, the economical and environmentally friendly diesel is the best choice for powertrains (Leonhard *et al.* [1]). Common rail systems having a solenoid injector is fed by a high pressure fuel pump. The pressure in the rail, as well as the start and end of the signal that activates the injector for each cylinder are

WIT Transactions on Engineering Sciences, Vol 89, © 2015 WIT Press
www.witpress.com, ISSN 1743-3533 (on-line)
doi:10.2495/MPF150351

electronically controlled. High injection pressure is the requirement of more efficient combustion. Until the mid 1980s diesel fuel injection systems for light vehicles operated at pressure of 300–400 bar (Beierer [2]). Today, modern CRS applications utilize maximum injection pressure of 2500 bar and above. More information about CRS can be found elsewhere (Ferrari *et al.* [3]).

Solenoid valves are used to control mass flow of fuel at injectors in a fuel injection system having a valve needle, the open and closed positions of which is controlled by the solenoid valve. The valve has a ball, which lifts up and opens a valve seat when current flows through the magnet assembly of the solenoid valve. Figure 1 shows a typical common rail fuel injector with electromagnetic fuel injection control (Seyken *et al.* [4]).

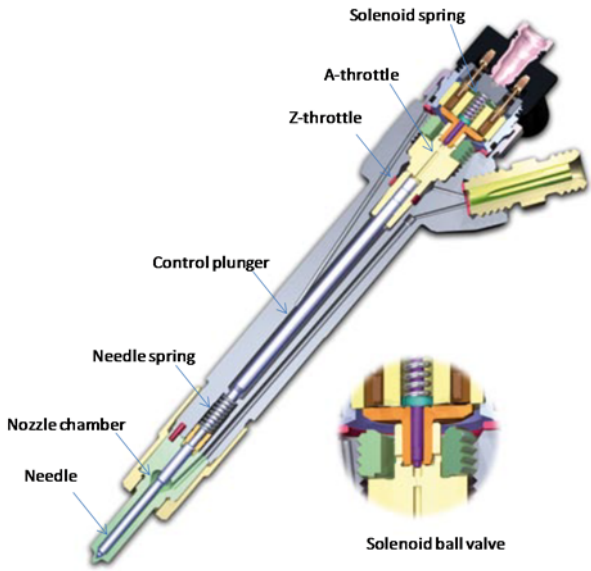

Figure 1: Cross section of Bosch common rail injector.

Solenoid valve of the injector flow shows characteristics of bubbly flow. In the valve seat region of solenoid valves the expansion of fuel flow from high pressure to low pressure regions creates bubbles. Cavitation erosion is caused by the extremely high pressure peaks that occur during the implosion of cavitation bubbles in the vicinity of seat wall (Brennen [5, 6]). The location of cavitation damage is dependent upon a variety of factors, including valve geometry and flow conditions at injectors. More discussion about cavitation process specific to diesel fuel injectors are available elsewhere (Martynov [7]).

Cavitation is observed in many hydrodynamic mechanical devices, such as pumps, turbines, nozzles and marine propellers, and can have an intensive effect on the performance of these devices. In solenoid valves cavitation bubbles formed especially over the surface of valve seat region cause material damage when these bubbles rupture. This is so-called cavitation erosion. However,

cavitating flow is also desired in solenoid valves due to the requirement of constant mass flow over the ball. Therefore, it is desired to understand its physics and to predict its erosive behaviour.

CFD modelling of cavitation requires two phase modelling due to generation of bubbles in diesel fluid flow within the solenoid valve geometry. Dirke *et al.* [8] described the cavitating flow with a two fluid model where liquid and vapour phase are treated separately. For each phase, a transport equation for the averaged volume fraction is used. It is reported that cavitation develops at the narrowest section of the valve seat. Delale *et al.* [9] presented mathematical theory and numerical simulation of bubbly cavitating unsteady quasi-one-dimensional nozzle flows.

Cavitation models are divided into the Lagrangian (discrete bubble) and Eulerian (continuum) approaches according to their computational framework Marjollet [10]. The Lagrangian approach focuses on the behaviour of discrete bubbles using bubble tracking and bubble dynamics equations Chahine [11]. The Eulerian approach is based on an approximation of a homogeneous mixture flow. The mixture flow moves at the same velocity, and each phase is identified by solving a volume fraction transport equation. The Eulerian approach was divided into the barotropic relation model [12–14] and two phase mixture flow model [15–18]. The barotropic relation model solves a single continuity equation with a barotropic relation equation between the pressure and density. On the other hand, the two-phase mixture flow model deals with two-phase continuity equations by employing a volume fraction transport equation. Unfortunately, the volume fraction contains no specific information on the shape or size of the cavitation entities in a volume cell (Dirke *et al.* [8]).

Kayakol [18] presented steady state and transient flow characteristics of bubbly diesel fluid flow in ball type solenoid valves. It is shown that stagnation effect due to deceleration of flow in front of the ball, detachment and re-attachment of flow along surface walls can be considered as key points in cavitation analysis due to their influence on bubble formation.

Cavitation erosion results from successive bubble collapse generating very high local pressures and temperatures. The initial incubation period of the material response to the erosion cavitation flow field does not involve any mass loss. With repeated impacts, hardening of the material surface layer develops, the deformation of the material accumulates, and finally micro-failures occur resulting in material removal and thus weight loss. A review of physical mechanisms and erosion risk models is available elsewhere (Terwisga [19]).

Commercial CFD codes provide a cavitation model but not a cavitation erosion model which deals with material damage of bubble collapse. Main parameters of conventional cavitation models, namely pressure and vapour volume fractions, indicate where bubbles are generated but do not explain how cavitation damage on material surfaces. Therefore, a cavitation erosion model needs to be used together with a cavitation model for the assessment of erosion.

In the present study, the cavitation erosion model, MDPR (Mean Depth Penetration Rate) is used as the quantification of the erosive potential of collapsing vapour structures. The cavitation erosion model runs at CFD post-

processing stage. The model (Franc [20]) is based on physical analysis of the work hardening process due to successive bubble collapses. The bubble interface velocity, which is assumed as micro-jet velocity, is calculated using Rayleigh–Plesset equation (Lin *et al.* [21]). Pressure impact of a bubble is also calculated for critical velocity which forms a pit [25] for the sake of comparison.

2 Cavitation model

A CFD analysis for solenoid valve of Bosch fuel injector is done for basic understanding of cavitation using ANSYS CFX V15.0 [22, 23]. Both bubble formation (evaporation) and collapse (condensation) are taken into account in the cavitation model of CFX which is based on the Rayleigh–Plesset equation (see Table 1). The cavitation model doesn't take thermal effects, turbulent kinetic energy, and surface tension into account. The k-ω shear stress transport SST model offers the best convergence situation especially for the cases having vortex formations.

Table 1: The cavitation model of CFX based on Rayleigh–Plesset equation.

Parameter	Definition	Eqn. No
The growth of a gas bubble in a liquid	$R_B \frac{d^2 R_B}{dt^2} + \frac{3}{2}\left(\frac{dR_B}{dt}\right)^2 + \frac{2\sigma}{\rho_f R_B} = \frac{p_v - p}{\rho_f}$	(1)
(Simplified Rayleigh-Plesset equation)	$\frac{dR_B}{dt} = \sqrt{\frac{2}{3}\frac{p_v - p}{\rho_f}}$	(2)
The rate of change of bubble volume	$\frac{dV_B}{dt} = \frac{d}{dt}\left(\frac{4}{3}\pi R_B^3\right) = 4\pi R_B^2 \sqrt{\frac{2}{3}\frac{p_v - p}{\rho_f}}$	(3)
The rate of change of bubble mass	$\frac{dm_B}{dt} = \rho_g \frac{dV_B}{dt} = 4\pi R_B^2 \rho_g \sqrt{\frac{2}{3}\frac{p_v - p}{\rho_f}}$	(4)
The volume fraction	$\alpha = V_B N_B = \frac{4}{3}\pi R_B^3 N_B$	(5)
Total interphase mass transfer rate per unit volume	$\dot{m}_{fg} = N_B \frac{dm_B}{dt} = \frac{3\alpha\rho_g}{R_B}\sqrt{\frac{2}{3}\frac{p_v - p}{\rho_f}}$	(6)
Condensation	$\dot{m}_{fg} = F_c \frac{3\alpha\rho_g}{R_B}\sqrt{\frac{2}{3}\frac{\lvert p_v - p\rvert}{\rho_f}}\,\mathrm{sgn}\left(p_v - p\right)$	(7)
Evaporation	$\dot{m}_{fg} = F_e \frac{3\alpha_{nuc}\left(1-\alpha\right)\rho_g}{R_{nuc}}\sqrt{\frac{2}{3}\frac{\lvert p_v - p\rvert}{\rho_f}}\,\mathrm{sgn}\left(p_v - p\right)$	(8)
Constants	$R_{nuc} = 1\ \mu\mathrm{m}$ $\alpha_{nuc} = 5\,\mathrm{E}-4$ $F_e = 50$ $F_c = 0.01$	

In the present study, the quantification of the erosive potential of collapsing vapour structures is based on the analytical model of Franc [20]. The equations of cavitation erosion model are given in Table 2.

Table 2: The equations used in CFX cavitation erosion model.

Growth rate of a cavitation bubble	$\dot{R} = \frac{\partial R}{\partial t} = \sqrt{\frac{2}{3}\frac{\lvert Pv - P\rvert}{\rho}}$	(9)
	$\dot{\alpha} = \frac{\partial \alpha}{\partial t} = \frac{3\,F_c \alpha}{R_{\max}}\left\lvert\frac{\partial R}{\partial t}\right\rvert$	(10)
Mean size of the impact zone	$S = \left(0.2R_{\max}\right)^2$	(11)
Pressure impact into the surface	$\sigma_1 = \rho c\left(-\frac{\partial R}{\partial t}\right)$	(12)
	$\varepsilon_1 = \left(\frac{\left(\rho c\left\lvert\frac{\partial R}{\partial t}\right\rvert - \sigma_e\right)}{K}\right)^{\frac{1}{\theta}}$	(13)
Thickness of the hardened layer	$l_1 = \left(\frac{\varepsilon_1}{\varepsilon_r}\right)^{\frac{1}{\theta}}$	(14)
Absorbed energy	$W_1 = l_1 S\varepsilon_1\left(\frac{\sigma_e}{(1-\theta)} + \frac{(K{\varepsilon_1}^m)}{(1+m)(1+(m+1)\theta}\right)$	(15)
Maximum of the absorbed energy	$W_1 = LS\varepsilon_r\left(\frac{\sigma_e}{(1-\theta)} + \frac{(K{\varepsilon_r}^m)}{(1+m)(1+(m+1)\theta}\right)$	(16)
Bubble number density	$\dot{n} = \frac{3\left(\frac{\partial \alpha}{\partial t}\right)}{4\pi R_{\max}^3}$	(17)
Bubble collapse intensity	$N = \dot{n}2R_{\max}$ $N = \left(\frac{3}{4\pi R_{\max}}\right)\underbrace{\left[\frac{3F_c\alpha}{R_{\max}}\sqrt{\frac{2}{3}\frac{\lvert P_v - P\rvert}{\rho}}\right]sign\,(P_v - P)}_{\text{Condensation rate}}$	(18)
Incubation time	$\tau = \frac{1}{N\bar{S}}\frac{W_u}{W_1}$	(19)
Mean displacement rate	$MDPR = LS^2N$	(20)

The method is based on physical analysis of the work hardening process due to successive bubble collapses. It is assumed that no mass loss appears and work hardening process occurs when stress acting on a material is greater than yield strength and weaker than the ultimate tensile strength of the material, and mass loss starts when cumulative energy of a material reaches the energy corresponding to the ultimate tensile strength.

In the MDPR model main parameters related to material side are yield strength, ultimate strength, and thickness of hardened layer. On the fluid side, the erosive potential of cavitating flow or flow aggressiveness is described in terms of the mean amplitude, rate, and mean size area of the hydrodynamic impact loads. The cavitation model is used for the calculation of flow aggressiveness. Predicted quantities of the model are given in Figure 2. As can be seen from the figure, parameters related to bubble dynamics are considered in the erosion model. Details of erosion model is described elsewhere (Kayakol [18]).

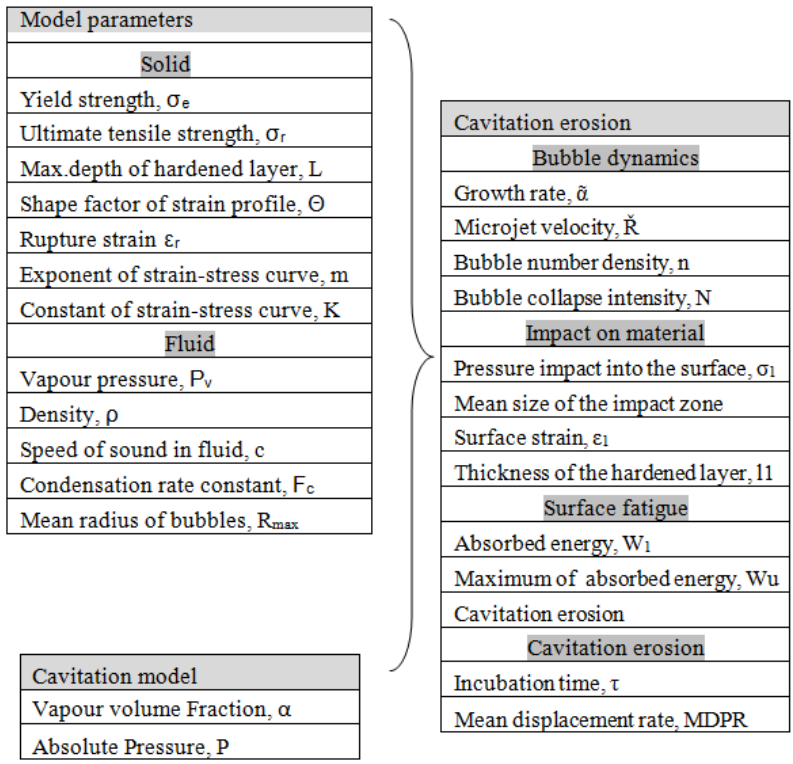

Figure 2: Predicted quantities of cavitation erosion model.

The collapse of a bubble near a wall generates a micro-jet that may not be modelled using the Rayleigh–Plesset equation which assumes spherical symmetry [24]. The critical velocity V_{crit} which forms a pit is defined as [25]

$$v_{crit}\sqrt{\frac{p_y}{\rho_l}\left(1-\left(1+\frac{p_y}{B}\right)^{-\frac{1}{n}}\right)} \tag{21}$$

where p_y= 300MPa and n=7.

2.1 Numerical setup

The liquid fluid and vapour properties are defined as "compressible diesel" and the vapour, respectively. The flow is considered at isothermal conditions. The numerical settings for the cavitation model are set to default values, except for the "Maximum Density Ratio", which is 32,000. The structured grid is generated with the ICEM–HEXA grid generation software.

2.2 Boundary conditions

At the boundaries of the domain pressure boundary conditions are applied. The back pressure is 1 bar and the inlet pressure is varied. The flow is considered at isothermal conditions with a constant temperature of 40°C.

3 Results and discussions

Comparison of non-cavitating and cavitating flow conditions can be done by comparing the contours of pressure scaled pressure between (0–1 bar) as shown in Figure 3. The figure on the left hand side indicates non-cavitating flow condition. There is a drastic pressure drop after flow restriction pipe and an increase in pressure below ball due to stagnation effect of the ball. The figure on the right hand side is a typical pressure contour of cavitating flow condition. There is a pressure increase along the surface of diffuser after flow restriction (a-throttle) due to flow detachment, compared to the case of non-cavitating.

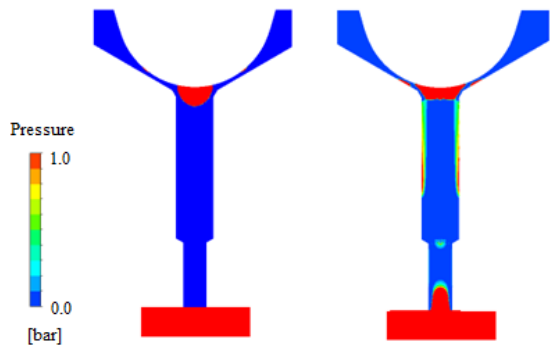

Figure 3: Contours of pressure scaled pressure between (0–1 bar) for (a) non-cavitating and (b) cavitating flow.

Figure 4 shows the plot of pressure versus distance along the line 1 (along wall) and line 2 (along centre). Pressure drops below vapour pressure of diesel, 30 mbar along line 1 and line 2. Then, pressure at line 2 increases due to stagnation effect of ball.

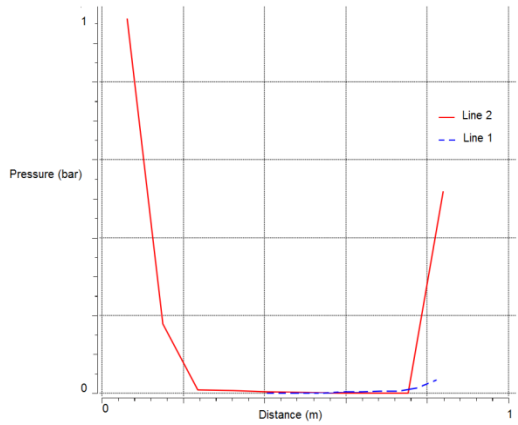

Figure 4: Plot of scaled pressure versus scaled distance along the line 1 (along wall) and line 2 (along centre).

The results of mixture type of cavitation model depend on selection of two parameters, condensation rate constant F_c and density ratio of diesel and diesel vapour. They affect assessment of cavitation erosion damage. The variation of MDPR and bubble collapse intensity in terms of condensation rate constant F_c is shown in Figure 5.

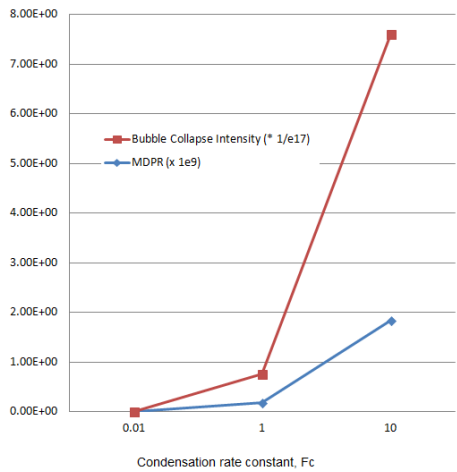

Figure 5: Variation of MDPR and bubble collapse intensity with condensation rate constant F_c.

As condensation rate increases more bubbles collapse and then bubble collapse intensity increases. The values of F_c are taken as 0.01, 1 and 10. In order to show MDPR and bubble collapse intensity on the same graph their values are multiplied with some numbers, as can be seen from the legend.

Since cavitation erosion is the result of the material response to repeated impact loads, it appears fundamental to accurately determine impact loads in order to be able to predict the erosion damage. The mean amplitude of pressure impact defined in Eqn (12) requires accurate prediction of micro-jet velocity. Table 3 shows variation of MDPR with cavitation bubble micro-jet velocities defined in Eqns (9) and (21). At lower micro-jet velocity the pressure impact to wall is less than material yield strength. But at higher micro-jet velocity the pressure impact to wall is less than material yield strength. This means that bubble collapse may cause plastic deformation. In addition, higher MDPR value is an indication of cavitation erosion.

Table 3: MDPR at different micro-jet velocities of a single bubble.

Micro-jet velocity (m/s)	Pressure impact (Pa)	MDPR
54 (Eqn. (9))	6.5e+7	1.8E-10
713 (Eqn. (21))	8.7e+8	2.4e-9

Figure 6 gives contours of vapour volume fraction at different density ratio of diesel and diesel vapour. The case with the density ratio of 10,000 produces liquid film near the wall of chamfer (see Figure 6(a)). However, the case with the density ratio of 32,000 produces vapour pocket near the wall of chamfer (see Figure 6(b)). Therefore, density ratio specific to case under consideration needs to be specified properly.

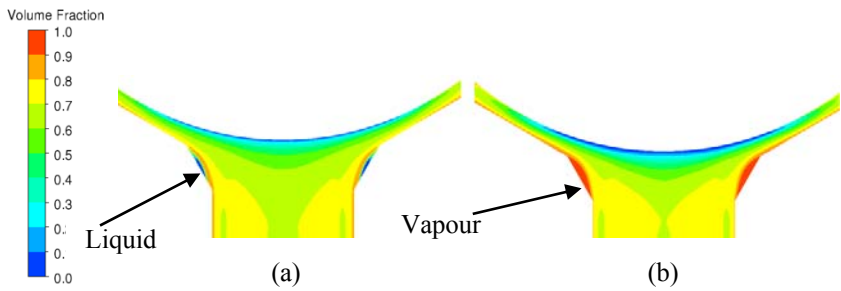

Figure 6: Contours of vapour volume fraction at density ratio of (a) 10,000 and (b) 32,000 for diesel and diesel vapour.

Figure 7 shows the plot of armature lift versus mass flow rate. Both the values of armature lift and mass flow rate are scaled between 0–1. In non-cavitating flow regime mass flow rate increases with armature lift linearly. Therefore, non-cavitating flow can be considered as single phase. As bubble formation increases with armature lift within the valve geometry mass flow remains constant.

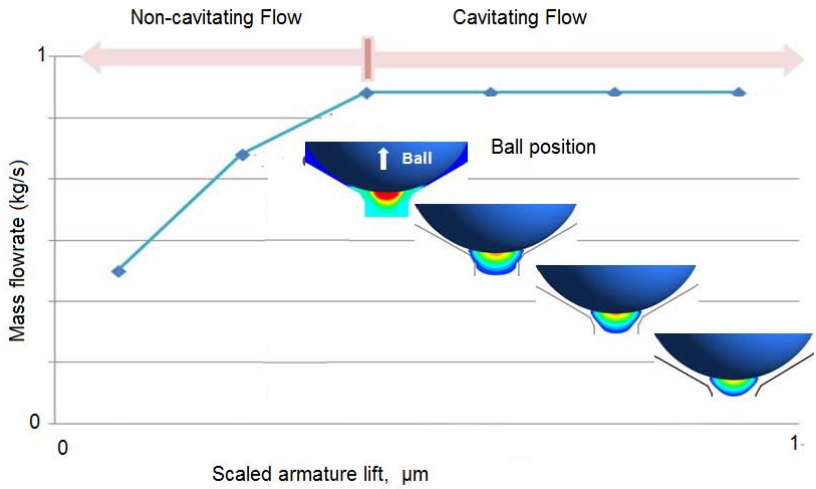

Figure 7: Scaled armature lift versus scaled mass flowrate.

In non-cavitating flow regime mass flow rate increases with armature lift linearly. Therefore, non-cavitating flow can be considered as single phase. As bubble formation increases with armature lift within the valve geometry mass flow remains constant. Cavitating flow shows two phase flow characteristics. Figure 10 also shows the contours of pressure at different ball position (i.e., armature lift). The high pressure below the ball occurs due to stagnation. As ball moves up stagnation region becomes away from surface. This means less cavitation erosion.

4 Conclusion

Cavitation erosion damage in solenoid valve for diesel common rail injectors is investigated with a two phase mixture model suited for bubble-liquid flow. The aim of investigation is not to avoid cavitation but control it so that bubbles collapse away from valve seat. The location of cavitation damage needs not only erosion mechanism but an accurate cavitation model which provides pressure and vapour distribution. However, the difficulty in CFD analysis of cavitating flow comes from the fact that the locations of bubble formation does not mean where bubbles implode. This is because bubbles form at low pressures but collapse at high pressure regions, especially below the ball and near valve seat. Pressure gain after throttling of high pressure fluid in the diffuser of solenoid valve is very poor due to micronized components of valve geometry.

Model parameters of a cavitation model based on Rayleigh–Plesset equation, especially condensation rate constant F_c and density ratio of diesel and diesel

vapour, need to be specified properly. The value of density ratio affects significantly vapour volume fraction distribution within the fluid medium.

It is shown that micro-jet velocity calculated from classic Rayleigh–Plesset equation is much lower than the micro-jet jet velocity that can cause a pit or plastic deformation on a material surface. Therefore, accurate calculation pressure impact calculated from Rayleigh–Plesset equation can be misleading.

References

[1] Leonhard, R., Pauer, T., Rückle, M. & Schnell, M., Solenoid common rail injector for 1800 bar. *MTZ Motortechnische Zeitschrift*, 71, pp. 10–15, 2010.

[2] Beierer, P., Experimental and numerical analysis of hydraulic circuit of a high pressure common rail diesel fuel injection system, *PhD*, Tampere University of Technology, Tampere, Finland, 2007.

[3] Ferrari, A., Mittica, A. & Spessa, E., Benefits of hydraulic layout over driving system in piezo-injectors and proposal of a new-concept CR injector with an integrated Minirail. *Applied Energy,* 103, pp. 243–255, 2013.

[4] Seyken, X.L.J., Modelling of common rail fuel injection system and influence of fluid properties on injection process, *Proceedings of VAFSEP*, Dublin, Ireland, 2004.

[5] Brennen, C.E., *Cavitation and bubble dynamics*. Oxford, UK: Oxford University Press, 1995.

[6] Brennen, C.E., *Fundamentals of multiphase flow*. New York, USA: Cambridge University Press, 2005.

[7] Martynov, S., Numerical simulation of the cavitation process in diesel fuel injectors, *PhD*, University of Brighton, UK, 2005.

[8] Dirke, M., Krautter, A., Ostertag, J., Mennicken, M. & Badock, C. Simulation of cavitating flows in diesel injectors. *Oil & Gas Science and Technology*, 54, pp. 223–226, 1999.

[9] Delale, C.F., Pasinlioglu, S. & Baskaya, Z., *Mathematical theory and numerical simulation of bubbly cavitating nozzle flows*. Springer–Verlag: Berlin, Germany, 2012.

[10] Marjollet, L.B., Specialist committee on cavitation, *Proceedings of 25th ITTC*, 3, Fukuoka, Japan, pp. 1–61, 2008.

[11] Chahine, G.L., Nuclei effects on cavitation inception and noise. *25th Symposium on naval hydrodynamic*, St. John's, Newfoundland and Labrador, Canada, 2004.

[12] Delannoy, Y. & Kueny, J.L., Two phase flow approach in unsteady cavitation modeling. *ASME cavitation and multiphase flow forum*, Toronto, Canada, 1990.

[13] Kubota, A., Kato, H. & Yamaguchi, H., A new modelling of cavitating flows: a numerical study of unsteady cavitation on a hydrofoil section. *Journal of Fluid Mechanics*, 240, pp. 59–96. 1992.

[14] Chen, Y. & Heister, S.D., A numerical treatment for attached cavitation. *Journal of Fluids Engineering*, 190, pp. 299–307, 1994.
[15] Schnerr, G. & Sauer, J., Physical and numerical modeling of unsteady cavitation dynamics. In: *4th International conference on multiphase flows*, New Orleans, LA, US, 2001.
[16] Singhal, A.K., Athavale, M.M., Li, H. & Jiang, Y., Mathematical basis and validation of the full cavitation model. *Journal of Fluids Engineering*, 124, pp. 617–624, 2002.
[17] Senocak, I., & Shyy, W., A pressure-based method for turbulent cavitating flow computations. *Journal of Computational Physics*, 176, pp. 363–368, 2002.
[18] Kayakol, N., CFD modelling on flow characteristics of two phase flow in solenoid valves. *Int. Symp. on Convective Heat and Mass Transfer*, CONV-14, Turkey, 2014.
[19] Terwisga, T.J.C., A review of physical mechanisms and erosion risk models, *Proceedings of the 7th International Symposium on Cavitation CAV2009*, pp. 17–22, 2009.
[20] Franc, J., Incubation Time and Cavitation Erosion Rate of Work-Hardening Materials. *Journal of Fluids Engineering*, 131, pp. 1–14, 2009.
[21] Lin, H., Storey, B.D. & Szeri1, A.J., Inertially driven inhomogeneities in violently collapsing bubbles: the validity of the Rayleigh–Plesset equation. *Journal of Fluid Mechanics,* 452, pp. 145–162, 2002.
[22] ANSYS CFX 15.0 Theory manual, ANSYS, Inc., 2014.
[23] Bakir, F., Rey, R., Gerber, A.G., Belamri, T. & Hutchinson, B., Numerical and experimental investigations of the cavitating behaviour of an inducer. *International Journal of Rotating Machinery*, 10, pp. 15–25, 2004.
[24] Kim, K., Chahine, G., Franc, J. & Karimi, A., Advanced experimental and numerical techniques for cavitation erosion prediction, France: Springer, 2014.
[25] Dular, M., Bachert, B., Stoffel B. & Sirok, B., Relationship between cavitation structure and cavitation damage, *Wear*, 257, pp. 1176–1184, 2004.